JOURNAL OF RAMAN SPECTROSCOPY
J. Raman Spectrosc. 2008; **39**: 1162–1169
Published online 31 March 2008 in Wiley InterScience
(www.interscience.wiley.com) DOI: 10.1002/jrs.1957

JRS

Thiol-immobilized silver nanoparticle aggregate films for surface enhanced Raman scattering

Carlos Caro,[1] Carlos López-Cartes,[2] Paula Zaderenko[1] and José A. Mejías[1]*

[1] Department of Physical, Chemical and Natural Systems, Universidad Pablo de Olavide, Carretera de Utrera Km 1, 41013 Sevilla, Spain
[2] Instituto de Ciencias de Materiales de Sevilla, CSIC-universidad de Sevilla, C. Americo Vespucio 49, 41092 Sevilla, Spain

Received 4 October 2007; Accepted 30 January 2008

We report a novel method for the fabrication of films of silver nanoparticle aggregates that are strongly attached to Si substrates (Thiol-immobilized silver nanoparticle aggregates or TISNA). The attachment is achieved by chemically modifying the surface of a Si(100) surface in order to provide SH groups covalently linked to the substrate and then aggregating silver nanoparticles on these thiol covered surfaces. The transmission electron microscopy (TEM), scanning electron microscopy (SEM) and atomic force microscopy (AFM) characterization show a high coverage with single nanoparticles or small clusters and a partial coverage with fractal aggregates that provide potential hot spots for surface enhanced Raman scattering (SERS). We have confirmed the SERS activity of these films by adsorbing rhodamine 6G and recording the Raman spectra at several concentrations. By using the silver-chloride stretching band as an internal standard, the adsorbate bands can be normalized in order to correct for the effects of focusing and aggregate size, which determine the number of SERS active sites in the focal area. This allows a quantitative use of SERS to be done. The adsorption–desorption of rhodamine 6G on TISNA films is reversible. These features make our TISNA films potential candidates for their use in chemical sensors based on the SERS effect. Copyright © 2008 John Wiley & Sons, Ltd.

KEYWORDS: immobilized metal nanoparticle aggregates; surface enhanced Raman spectroscopy; substrates for SERS spectroscopy; silver nanoparticles; SEM; TEM; AFM

INTRODUCTION

Thin films of nanostructured materials are of great interest due to their potential for novel applications in chemical sensing,[1] nanoelectronics,[2] optical devices,[3] ... etc. Among these systems, metal films with controlled nanostructure and composition are intensely investigated due to their interesting physical and chemical properties.[4,5] One of their most important applications is surface enhanced Raman scattering (SERS).[6] It is well known that many molecules adsorbed on certain metal substrates increase their Raman cross section by several orders of magnitude, from 10^2 in the more modest cases to even 10^{14} for some molecule-surface combinations. SERS is the base of many studies that aim at reaching ultrasensitive detection for a wide range of compounds ranging from simple chemical pollutants to biomolecules and immunoassays.[7–9] In many of these studies the detection of even a single molecule has been reported.[10]

*Correspondence to: José A. Mejías, Department of Physical, Chemical and Natural Systems, Universidad Pablo de Olavide, Carretera de Utrera Km 1, 41013 Sevilla, Spain.
E-mail: jamejrom@upo.es

There are also several attempts to develop quantitative or semiquantitative SERS methods,[11–16] some of them based on the use of internal standards[17]. Two general mechanisms have been proposed for SERS namely (1) the electromagnetic enhancement and (2) the chemical effect. In (1) the excitation of surface plasmons of the metal nanostructures leads to the amplification of the electromagnetic fields at certain regions near their surfaces, which results in enhanced excitation and emission. In (2) the molecule-metal interaction leads to new electronic states that are excited by the incident laser light, which results in enhancement such as in resonant Raman scattering. In order for either or both of these mechanisms to play a role, one needs the metal substrate to have certain characteristics especially as far as its nanostructure is concerned. First, the most active metals for SERS seem to be copper, silver and gold due to their surface plasmon resonances that can be excited with visible light, with silver having a prominent role. Second, the metal needs to be rough at the nanoscale, with sharp edges and kinks and or being made of nanoparticles, nanoislands, ... etc. Also, the presence of gaps of a few nanometers between nanoparticles, the so called hot spots, cause a huge enhancement of

the electromagnetic fields. These hot spots are mainly responsible for large SERS effect in many cases. There is a variety of methods for the fabrication of SERS substrates, such as metal evaporation,[18,19] chemical or electrochemical etching or deposition on smooth surfaces[20] and deposition or assembly of metal nanoparticles from solution.[21] Within that last set of methods, the use of aqueous metal colloids that are assembled on a substrate is widespread since the synthesis of metal nanoparticles in solution does not require high vacuum nor other specialized equipment. There is also a variety of methods for assembling these nanoparticles on a substrate. The simplest one is the deposition of a droplet of colloid and further evaporation of the solvent.[21] Quite often, the colloid is aggregated and/or activated by addition of a salt and the result is the formation of nanoparticle aggregates on a solid support such as simply a glass slide. Owing to its simplicity and presence of hot spots, this method has been widely used and many applications have been reported including detection of pollutants,[22] dyes[23] and biomolecules.[1,13,24,25] Despite being widely utilized, the aggregation of metal colloids on a substrate has several disadvantages such as the lack of reproducibility and lack of stability due to the weak interaction between the nanoparticles and the substrate. Other more recent SERS active substrates are prepared by placing a layer of charged polymer and then putting down silver nanoparticle aggregates that are anchored by electrostatic forces. In most of these works, silver or gold nanoparticles are anchored to adsorbates of varying chemical nature but always contain amine groups.[26–30] There are works in which silica nanoparticles are functionalized with different silanes containing amine, thiol or hydrophobic groups. Small gold clusters are then attached to the functionalized particles and the effect of functionalization on gold adsorption and aggregation is studied.[31] We are not aware of any more recent work on the anchoring of silver nanoparticles through thiol groups, or a combination of them with amine groups.

In this work, we report a novel method for the fabrication of SERS active substrates in which the silver nanoparticle aggregates are strongly attached to the substrate by means of thiol groups that are covalently bonded to the support. The thiol groups are anchored to a Si(100) substrate through simple coupling chemistry involving primary amine groups that turn into amides and that remain in the functionalizing layer. Thus, a combined effect of thiols and amides on the nanoparticle attachment and aggregation is most likely. These nanostructures are characterized by means of transmission electron microscopy (TEM), scanning electron microscopy (SEM) and atomic force microscopy (AFM). The SERS activity has been studied by adsorbing rhodamine 6G, R6G, and then recording the spectra in a Raman microscope. Our procedure leads to Si substrates that are fully covered with single silver nanoparticles or small clusters. That layer of more disperse nanoparticles is partially covered with fractal like aggregates with sizes that range from one or two microns, to a few tens of microns. We distinguish two types of aggregates. On the one hand, about 90% of the aggregates are rather flat, with heights of a few tens of a micron at the most. On the other hand, ≈10% of the aggregates are thicker and spherical like. All these fractal aggregates are SERS active, with a large number of hot spots for enhancement, as well as rather stable, reproducible and reversible, owing to the strong attachment of the aggregates to the support. Most of our Raman spectra are recorded with a 785 nm laser that is more convenient in order to avoid unwanted fluorescence from the adsorbates. Some measurements are also done by exciting with a 532 nm laser in order to have a stronger enhancement since the plasmon resonances of the silver nanoparticles are centered at a wavelength of about 415 nm. We also report some preliminary results that point to the feasibility of performing quantitative SERS by rescaling the Raman signals to take into account factors such as aggregate size or variability due to focusing of the sample.

EXPERIMENTAL

Materials

All the chemicals are of reagent grade and have been used without further purification: (N-(3-dimethylaminopropyl)-N′-ethylcarbodiimide hydrochloride (EDC) Chemical abstract service (CAS) = 25952-53-8, hydroxylamine hydrochlorure CAS = 5470-11-1, mercaptoacetic acid (MAA) CAS = 68-11-1 and rhodamine 6G (R6G) CAS = 989-38-8 from Sigma Aldrich. N-hydroxisuccinimide (NHS) CAS = 6066-82-6 and potassium nitrate CAS = 7757-79-1 and 2-(N-morpholino)ethanesulfonic acid 1-hydrate (MES) CAS = 224-632-3 from Panreac. (3-aminopropyl)trimethoxysilane CAS = 25952-53-8 from Alfa-Aesar. Water was purified using a Milli-Q reagent grade water system from Millipore. As substrates for immobilization, we use high purity and high resistivity silicon wafers from Topsil. These wafers are polished on both sides and with (100) orientation.

Immobilization of nanoparticles on Si substrates

The method for immobilization of aggregated nanoparticles is depicted in Fig. 1. We begin by oxidizing the Si(100) surface in a freshly prepared piranha solution (H_2O_2 : H_2SO_4 1: 3) for 1 h. This results in the formation of a silanol covered SiO_2 layer that is then reacted with (3-aminopropyl)trimethoxysilane for 2 h in order to form an amine terminated layer. This film is then immersed for 2 h in a MES buffer solution containing MAA that has been activated with EDC + NHS and that couples with the amine layer. This provides a substrate that is covered with SH groups that, upon immersion during 1 h in a suspension of silver nanoparticles that are being aggregated in KNO_3 10^{-2} mol/l, are covered by a layer of nanoparticles that are strongly attached to the substrate. The silver nanoparticles are formed by reduction of $AgNO_3$ with hydroxylamine following the

DOI: 10.1002/jrs

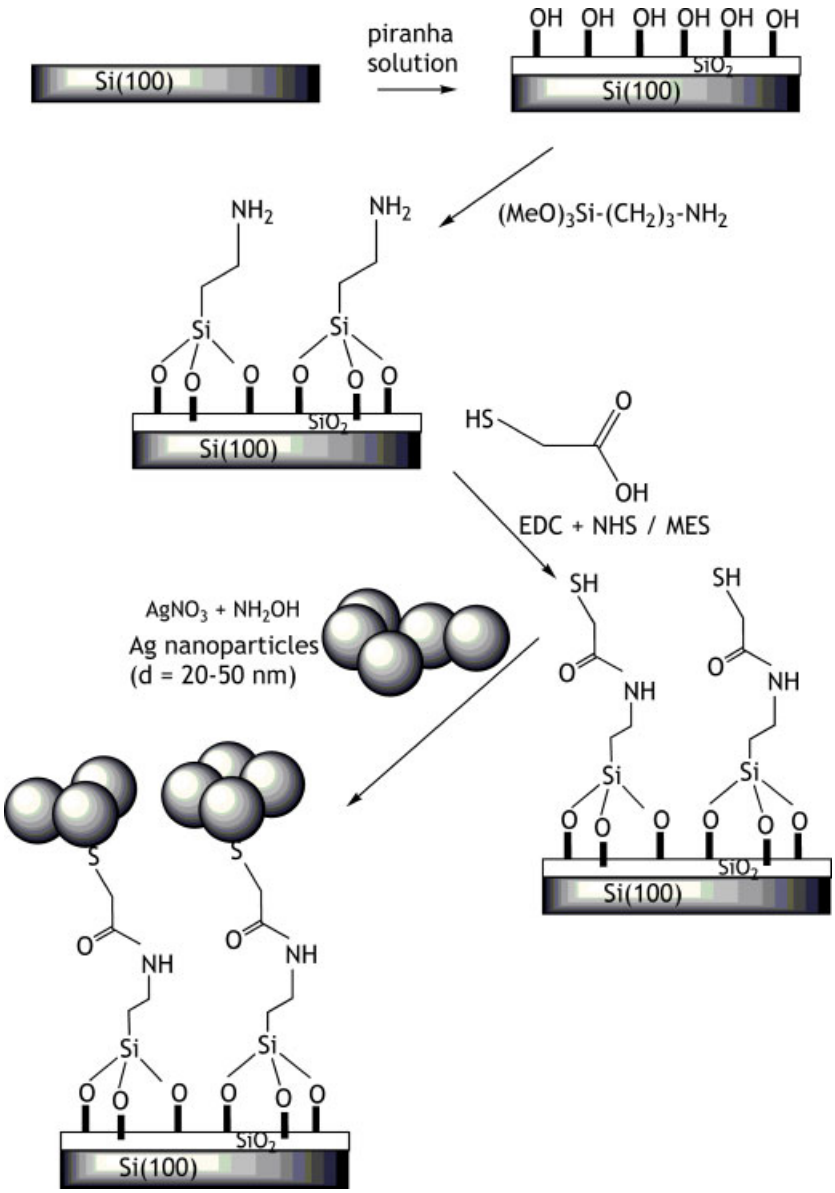

Figure 1. Scheme of the method used for the formation of the TISNA films on a Si(100) surface as explained in the text. This figure is available in colour online at www.interscience.wiley.com/journal/jrs.

method of Leopold and Lendl.[32] After each of these steps, the films are washed thoroughly during 1 h in Milli-Q water.

Atomic force microscopy

AFM images were obtained with a Molecular Imaging Pico Plus instrument working in tapping mode, a scanner of 10 μm × 10 μm and a silicon cantilever.

Transmission Electron Microscopy (TEM)

TEM images were taken using a Philips CM200 microscope. The samples under study were prepared by drying a drop of an aqueous solution of nanoparticles on a copper grid coated with a carbon film.

Scanning Electron Microscopy (SEM)

SEM images were obtained with a Hitachi S5200 high resolution microscope.

UV-Vis spectroscopy

Absorption spectra were recorded with an Ocean optics spectrometer equipped with a HR4000 detector.

Raman spectroscopy

The samples for Raman spectroscopy were prepared by dipping the nanoparticle layers in R6G aqueous solutions of several concentrations and drying them with nitrogen at room temperature. SERS spectra were measured in a Bruker Senterra Confocal Raman Microscope equipped with

DOI: 10.1002/jrs

a 785 nm laser. We make use of the 50× objective for all the measurements, the slit aperture is fixed to 50 μm and the integration time is 100 s with a laser power of 10 mW. All the spectra are recorded with a 3 cm^{-1} resolution. For the Raman measurements with a laser at 532 nm, we make use of a Horiba Jobin Yvon HR 800 UV spectrometer with a 50× objective a laser power of 10^{-5} mW, an integration time of 1 s a slit aperture of 100 μm and a resolution of 3 cm^{-1}.

RESULTS AND DISCUSSION

The reduction of $AgNO_3$ in aqueous solution with $NH_2OH \bullet HCl$ yields chloride protected Ag polyhedral nanoparticles with typical sizes between 20–50 nm as determined by TEM (Fig. 2). The aqueous colloidal suspensions of these particles have a plasmon resonance at 415 nm in the UV-Vis absorbance spectrum (not shown).

The initial treatment of the Si(100) surface with piranha solution leads to a SiO_2 layer that can be detected by Fourier transform infrared (FTIR), with clearly visible bands centered at 1045 cm^{-1} and 1149 cm^{-1} as shown in Fig. 3. These bands are assigned to SiO_2 transverse-optic (TO) oxygen asymmetric (AS_1 and AS_2) stretch modes.[33] A new band also appears at 895 cm^{-1}, which we assign to the Si–H stretching in O_3SiH configurations.[34] The FTIR spectrum displays other bands at 1700 cm^{-1} and 2200 cm^{-1} that are probably due to the presence of water that is adsorbed rapidly as the sample is transferred from a dry nitrogen atmosphere to the FTIR chamber. There is also a broad feature between 2600 cm^{-1} and 3600 cm^{-1} from υ(OH) modes of strongly hydrogen bonded water and SiOH groups. The comparison between this spectrum and the one of bulk water (acquired in ATR mode) shows clearly that the SiO_2 TO bands are distinct from water bands, which confirms that an oxide layer appears after the treatment with piranha solution. That layer is hydrophilic, most likely due to the presence of a large number of silanol groups such as required for the effective coupling of the silane and then the activation with SH groups. The rest of these chemical changes on the substrate cannot be detected by transmission FTIR probably due to the weakness of the signals.

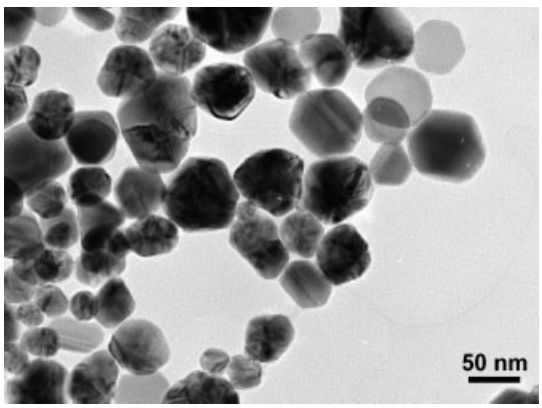

Figure 2. TEM image of the Ag nanoparticles synthesized using $AgNO_3$ and $NH_2OH{\cdot}HCl$.

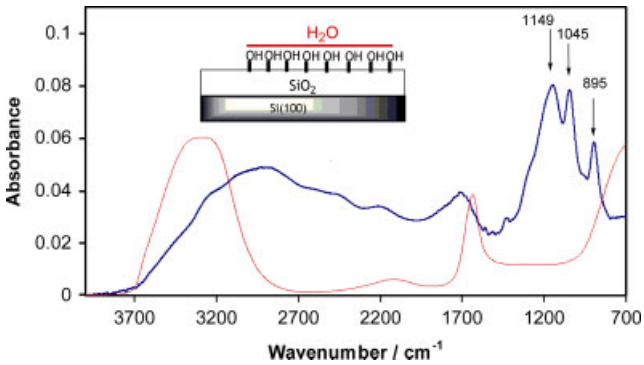

Figure 3. Transmission FTIR spectrum of the Si(100) chip after treatment with piranha solution for 1 h. The sample has been rinsed in MilliQ water and dryed with nitrogen. The spectrum of liquid water, recorded in a 10 reflection ZnSe ATR, is also shown for comparison as discussed in the text. This figure is available in colour online at www.interscience.wiley.com/journal/jrs.

Figure 4 shows three different SEM images of the nanoparticle covered substrates. Figures 4(A) and (B) show a high coverage degree with nanoparticle aggregates of different sizes, ranging from what probably are single particles or small clusters that seem to cover the whole surface, to large fractal-like aggregates that cover from several μm^2 to a few tens or even a few hundred μm^2 on some areas. The high resolution images (Fig. 3C) show that all these clusters comprise numerous sites with rather small gaps between nanoparticles, which are just a few Angstroms apart. These sites may act as hot spots for enhancement of electromagnetic fields as required for SERS.

The AFM images show that the height of most of these aggregates, ≈90%, is limited to several tenths of a micron at the most. For example, the AFM image in Fig. 5 shows a typical aggregate that cover an area of ≈1 μm^2 and a height of only about 0.2 μm. It is also possible to focus the top of these flat aggregates along with the substrate in the optical microscope. This flat character of the greater part of aggregates is probably caused by the strong interaction between the aggregating nanoparticles and the thiol covered surface. There is a minor presence of some spherical-like thick aggregates. Each of them covers an area similar to the flat ones. Although we have been unable to characterize the exact topography due to the limitations of the AFM scanner, we estimate that these aggregates are at least ten times higher than the flat ones. For example, it is not possible to focus the whole of a thick aggregate nor is it possible to focus the top and the substrate at the same time in the optical microscope, which suggests a height of a few microns. Presumably the flat aggregates have grown on the substrate so that the nanoparticle-surface interaction has determined their shape, whereas the more spherical

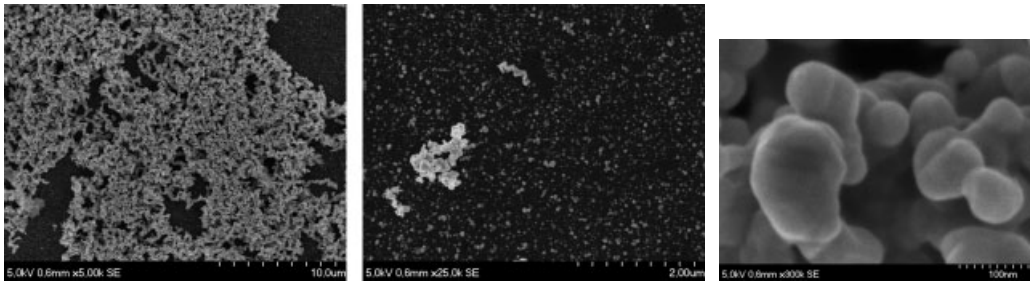

A B C

Figure 4. SEM images of the thiol-covered Si(100) surfaces after exposure to the aqueous suspension of nanoparticles and then washed thoroughly in ultrapure water. (A) Large aggregate that covers an area of several hundred of μm^2. (B) Layer of sparse nanoparticles or small nanoparticle clusters and a small flat aggregate. (C) Higher resolution image of part of the small aggregate in B that shows several particles and the gaps that may act as hot spots for SERS.

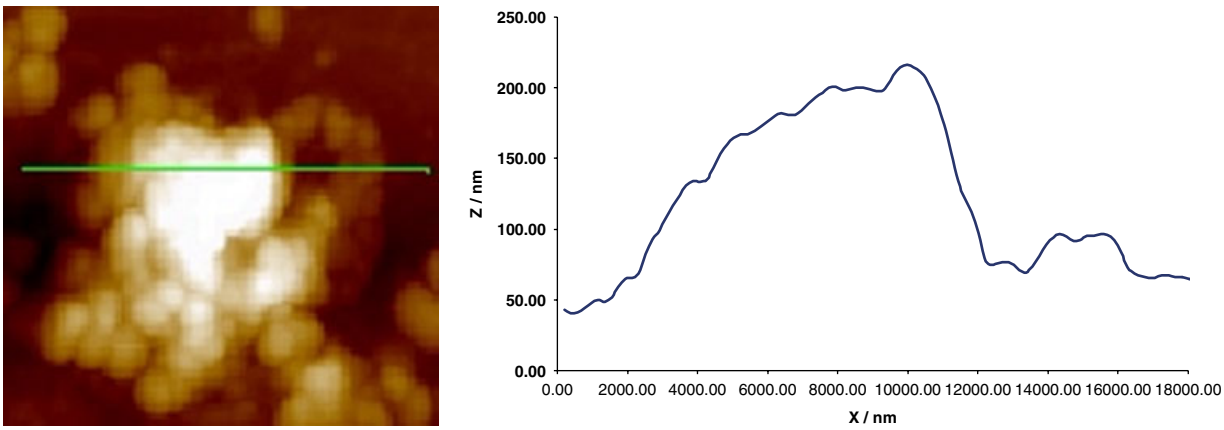

A B

Figure 5. (A) AFM image of a small aggregate, slightly larger than the one shown in Fig. 3(B). The picture shows an area of 2 μm × 2 μm. (B) Height, Z, profile along the path, X, along the green line shown in A. This figure is available in colour online at www.interscience.wiley.com/journal/jrs.

aggregates have been formed in solution and then adsorbed. All these structures are rather stable on the substrate and remain unaltered after washing for several hours in Milli-Q water. Although we attribute all these features to the strong interaction between silver aggregates and the thiol groups at the modified surface, we think that it is also likely that the presence of protonated amine groups, from the silane sites that remain unreacted after the coupling of carboxylic groups, contributes significantly to such a strong interaction.

After incubating the nanoparticle films in 10^{-3} M, 10^{-4} M, 10^{-5} M, 10^{-6} M and 10^{-7} M solutions of R6G for 1 h and then drying them quickly under a stream of pure nitrogen, the silicon slides are observed in the optical microscope, with no apparent change in morphology. In Fig. 6, we show the SERS spectra obtained by focusing different spots on the sample. The Raman spectrum of the zones that are covered with single particles or small clusters do not yield appreciable signal from R6G and only the Raman peak of Si at 522 cm^{-1} is observed. In order to record Raman scattering from R6G, it is necessary to focus a nanoparticle aggregate. Flat aggregates, such as A in Fig. 6, with only one or two layers of particles as measured with AFM, show clearly the R6G signal. The fact that aggregate A is a flat one can also be easily checked because the substrate and the top of the aggregate lie nearly in the same focal plane. By focusing the top of thick aggregates (B and C in Fig. 6) one records a considerably stronger signal, although aggregate A also yields a rather clear spectrum with several R6G bands[21,27,35] at 611 cm^{-1}, 770 cm^{-1}, 1190 cm^{-1}, 1310 cm^{-1}, 1354 cm^{-1}, 1504 cm^{-1}, and 1593 cm^{-1}. The band at 522 cm^{-1} observed in spectrum A that has been enlarged 40 times, A × 40 in the figure, is assigned to the Si substrate. That band is absent for aggregates B and C since the substrate plane is clearly defocused. There is also a band at 230 cm^{-1} that is assigned to the Ag–Cl stretching at the surface of the chloride protected particles.[22]

It is noteworthy that the R6G spectra obtained from flat aggregates are better resolved, with narrower bands,

DOI: 10.1002/jrs

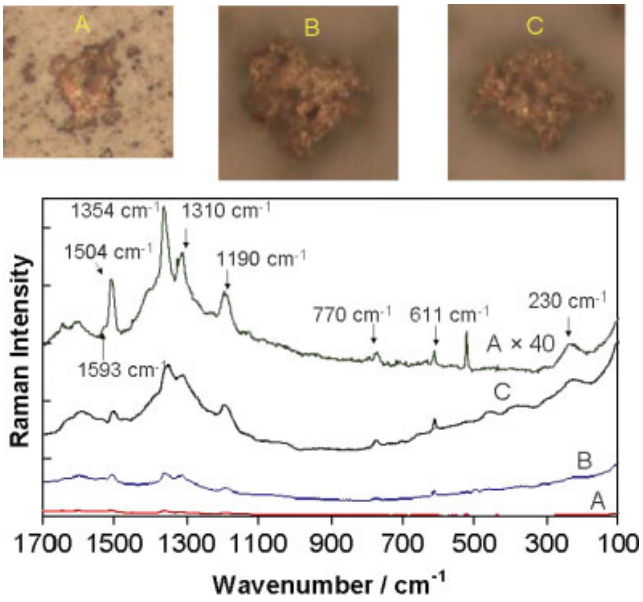

Figure 6. Top: 20 μm × 20 μ optical images of different nanoparticle aggregates dipped in 1 mM R6G and then dried in nitrogen. (A) flat aggregate that is in the same focal plane as the substrate, (B) and (C). Images of the top of larger aggregates focused several microns above the substrate. Bottom: SERS spectra recorded for spots centered in the aggregates A, B and C shown in the pictures. The spectrum of aggregate A amplified 40 times, A × 40, is shown in order to make the R6G bands visible in the same scale that is used for spectra B and C. This figure is available in colour online at www.interscience.wiley.com/journal/jrs.

than the spectra measured on thick aggregates. Compare for example the bands at 1310 cm^{-1}, 1354 cm^{-1} and 1593 cm^{-1} in spectrum A × 40 to the same bands in spectrum C in Fig. 6.

Clearly the intensity of the Raman signal measured for a given aggregate depends on the amount of SERS active spots in the focused volume. For example, when recording the spectrum from a flat aggregate the focused cylinder must contain a smaller number of hot spots than when focusing a thick one. For this reason, it is not feasible to relate the intensity of the Raman signal with concentration by using the as recorded spectra. Such a drawback can be overcome by rescaling all the spectra so that they all have the same area under the band centered at 230 cm^{-1}, the Ag–Cl stretching, since such area must be proportional to the number of nanoparticles in the focal region. This rescaling is shown in Fig. 7(A) for the different R6G concentrations used here. Clearly the intensity of the R6G bands increase with concentration once the spectra have been rescaled. Such a relationship has prompted us to calculate the ratio of areas under the R6G bands and the area under the υ(Ag–Cl) band and then to correlate them to concentration. Such a kind of correlation could be the basis for a quantitative use of SERS by using these substrates with a range of aggregate sizes. In order to test this idea we have calculated the areas, A_1, under the R6G bands centered at 1310 cm^{-1} and 1354 cm^{-1} by integrating the spectrum between 1281 cm^{-1} and 1391 cm^{-1}. Then we have calculated the area, A_2, under the υ(Ag–Cl) band, by integrating between 177 cm^{-1} and 322 cm^{-1}. Finally we have plotted the normalized area, A_1/A_2, *vs* concentration. We find that the data shows a linear dependence in a log–log plot such as shown in Fig. 7(B).

Thus, the following equation has been used to fit the data

$$A_1 \Big/ A_2 = \alpha\, C^{\beta}$$

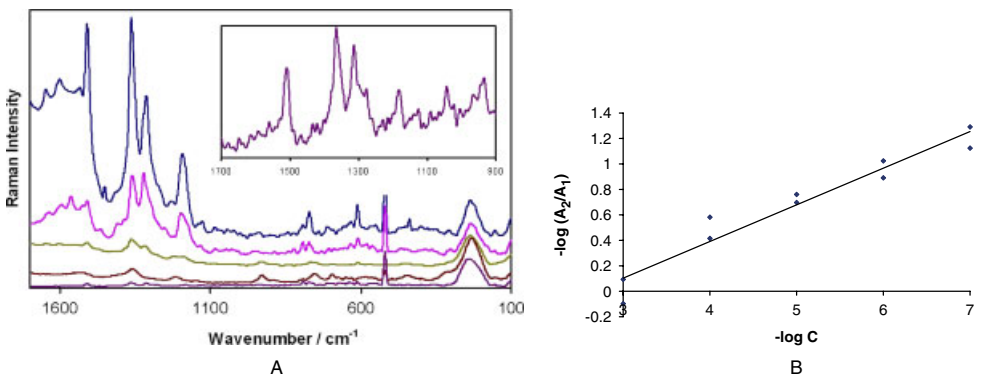

Figure 7. (A) SERS spectra taken by focusing flat aggregates on TISNA films that have been dipped for 1 h in R6G solutions of increasing concentration. From bottom to top: 10^{-7} M, 10^{-6} M, 10^{-5} M, 10^{-4} M, and 10^{-3} M. The inset shows the amplified spectrum for C = 10^{-7} M in the region of the main R6G bands. All the spectra have the base line removed and then have been rescaled so that they all have the same area under the υ(Ag–Cl) band at ≈230 cm^{-1}, A_1, calculated by integrating between 177 cm^{-1} and 322 cm^{-1}. (B) Log–log plot of the normalized area, A_2, of the 1310 cm^{-1} plus 1354 cm^{-1} bands, integrated from 1281 cm^{-1} to 1391 cm^{-1}, *vs* molar concentration. We have included two points for each concentration, one for a flat aggregate and another point for a spherical like aggregate. The best straight line fits to these points is $-\log(A_2/A_1) = -0.288\ \log\ C - 0.762$ with $R^2 = 0.937$. This figure is available in colour online at www.interscience.wiley.com/journal/jrs.

DOI: 10.1002/jrs

where A_1 and A_2 are defined above, C is molar concentration and α and β are fitting parameters that are calculated from a line fit in the log–log plot. β is a dimensionless parameter whereas α has dimensions of concentration$^{-\beta}$ The values that fit our data are $\alpha = 0.762\ \mathrm{M}^{-0.288}$ and $\beta = 0.288$. The line fit in Fig. 7(B) has $R^2 = 0.934$, which is a surprisingly good result given the huge range of concentrations of R6G, from 10^{-7} M to 10^{-3} M. Other authors have found linear dependences between intensities of SERS lines and concentration,[12] although for a range of concentrations that is considerable smaller than in this work.

It is noteworthy that in our R6G SERS experiments, the thiol-immobilized silver nanoparticle aggregates (TISNA) films are able to work reversibly, a feature that makes them reusable. In Fig. 8, we display three spectra recorded by focusing medium size spots on the same reused film. Spectrum A, for the film incubated in R6G 10^{-7} M for 1 h, shows clearly the R6G bands, spectrum B was taken after washing for 1 h in ultrapure water and does not show any SERS signals from R6G, finally, spectrum C, recorded after re-incubating in R6G 10^{-7} M, shows clearly a R6G fingerprint that is rather similar to that in the initial spectrum. These spectra illustrate that our TISNA films can work reversibly, a feature that would be desirable for their integration in sensors based on SERS.

Finally, one may speculate whether the Raman spectra reported here are true SERS spectra or simply nonenhanced Raman spectra or even fluorescence signals from R6G. One argument against the SERS effect is that the laser wavelength used here, 785 nm, is far off the plasmon resonance of the single particles, centered at about 415 nm. This has prompted us to record Raman spectra of the films incubated in R6G by using a 532 nm laser, since that shorter wavelength will excite the plasmon resonances and the electromagnetic enhancement will play a more important role. In Fig. 9, we compare one of such spectra to the equivalent spectrum recorded by exciting at 785 nm. The integration time for the 532 nm spectrum is 1 s only whereas for the spectrum obtained exciting at 785 is 100 s. Even so the former spectrum is about 100 times stronger that the 785 nm one. Thus, the Raman intensity recorded at 532 nm is about 10^4 times more intense that at 785 nm. This supports that we are recording true metal enhanced Raman spectra. Also the fact that R6G absorbs light at about 500 nm, with negligible absorptivity at 785 nm, also suggests that the fluorescence of R6G has little or no contribution in our measurements.

We also think that it is unlikely that the Raman spectra of R6G adsorbed on nanoparticle aggregates are not a simple effect of the large surface area of these aggregates. This has confirmed that by recording spectra from aggregates of nonmetal nanoparticles with similar sizes to those of silver nanoparticles. For example, adsorption of R6G on aggregated and sintered P25 TiO_2 nanoparticles does not produce any measurable Raman signal by exciting with the 785 nm laser. Even by incubating at 10^{-3} M R6G solutions, that yields stained TiO_2 aggregates, the Raman signals are not detectable. Thus, the results here reported are true surface enhanced Raman spectra of R6G adsorbed on nanoparticle aggregates.

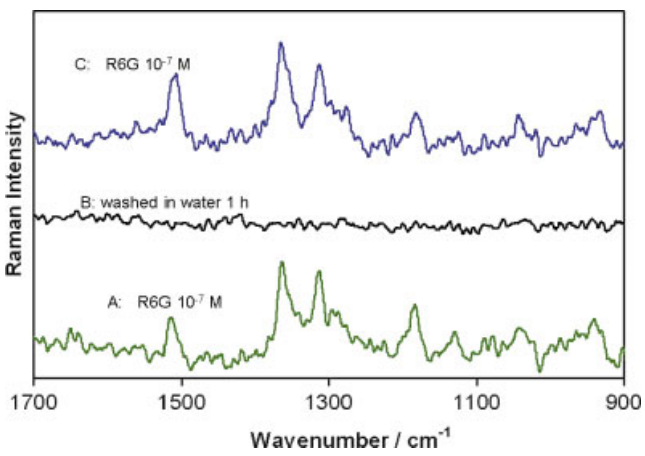

Figure 8. SERS spectra recorded on the same TISNA film after, (A) incubating it in R6G 10^{-7} M for 1 h, (B) thorough washing in Milli-Q water for 1 h and, (C), re-incubating it in R6G 10^{-7} M. This figure is available in colour online at www.interscience.wiley.com/journal/jrs.

CONCLUSIONS

We have reported the preparation of TISNA films on Si(100) substrates. The Si(100) surface is chemically modified in a simple 4-step process including aqueous phase reactions in piranha solution, adsorption of a silane that provides amine groups and coupling of MAA by means of a

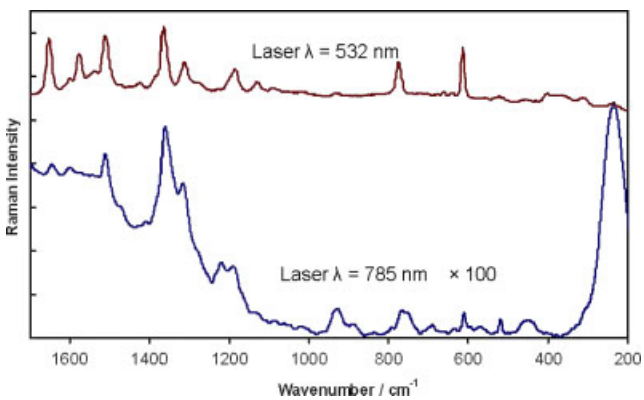

Figure 9. Raman spectra recorded on a TISNA film that has been incubated in R6G 10^{-5} M. Top spectrum has been recorded by using a 532 nm laser and 1 s integration time. Bottom spectrum with a 785 nm laser and 100 s integration time. In this figure bottom spectrum has been multiplied by 100 in order to fit the same scale as the top spectrum. This figure is available in colour online at www.interscience.wiley.com/journal/jrs.

DOI: 10.1002/jrs

carbodiimide, EDC. Finally silver nanoparticles, including nanoparticle aggregates formed under the presence of KNO_3, are deposited on the modified surface. The films obtained with this method, characterized mainly by SEM and AFM, consist of a layer of single particles of small aggregates covering fully the activated surface, plus a large number of aggregates. Each of these aggregates covers from just a few up to a few hundred of μm^2 on the surface. Most of the aggregates are rather flat in character, whereas a minor part of them, ≈10%, are more spherical like and thicker. Presumably the flat structures have grown by aggregation of nanoparticles on the substrate while the thick ones have been formed in solution and then have been attached to the surface. These TISNA films are rather stable and do not change appreciably by washing them thoroughly in ultrapure water.

The SERS activity of these films has been studied for adsorbed R6G in a range of concentrations from 10^{-3} M to 10^{-7} M. R6G SERS spectra have been recorded on both types of aggregates, flat and thick, with no SERS signal from the sublayer of more disperse particles. Even the thinner aggregates provide the hot spots that make good quality spectra possible to record, with a high signal-to-noise ratio, of R6G for films that have been incubated in aqueous 10^{-7} M solutions. Interestingly, thin aggregates seem to provide narrower bands than the spherical like aggregates, although the second ones provide considerably more intense spectra. For a given TISNA film and a given R6G concentration, the intensity of the SERS spectrum depends on the number of hot spots that lie within the focused area. We have investigated the feasibility of rescaling the spectra so that all they have the same area under the Ag–Cl band, which is proportional to the number of nanoparticles in the aggregate or the number of hot spots, so that the intensity under the R6G bands can be related directly to concentration. We think that the use of the υ(Ag–Cl) band as an internal standard is particularly interesting and deserves a more detailed study since it is considerably simpler than using other internal standards such as isotope edited species.[17] Our preliminary results show that there is a linear correlation between the rescaled area and concentration in a log–log plot. These results, together with the re-usability and reversibility as well as the stability of these TISNA films, make them suitable candidates for their use in chemical sensors bases in the SERS effect.

Acknowledgements

This research is funded by Spanish ministry of Education and Science (grant number CTQ-2004-00582), Spanish Ministry of Environment (grant numbers 644/2006/3-11.5 and A599/2007/3-11.5) and 'Confederación Hidrográfica del Guadalquivir' (CHG) under agreement between CHG and UPO for 2007. We thank Dr C. Cerrillos (CITIUS, University of Sevilla) for obtaining AFM images. We thank Dr Juan Carlos Sánchez López for his assistance in recording the Raman spectra with the 532 nm laser.

REFERENCES

1. Huang XJ, Choi YK. *Sensr. Actuators B-Chem.* 2007; **122**: 659.
2. De Micheli G. *Lect. Notes Comput. Sci.* 2006; **4148**: 658.
3. Novotny L, Hecht B (eds). *Principles of Nano-Optics*. Cambridge University Press: Cambridge, 2006.
4. Shalaev VM, Kawata SE. *Nanophotonics with Surface Plasmons*. Elsevier: Amsterdam, 2007.
5. Feldheim DL, Foss CAJE. *Metal Nanoparticles. Synthesis, Characterization and Applications*. Marcel Dekker: New York, 2002.
6. Kneipp K, Moskovits M, Kneipp H (eds). *Surface-Enhanced Raman Scattering. Physics and Applications*. Springer-Verlag: Berlin Heidelberger, 2006.
7. Kneipp K, Kneipp H. *Can. J. Anal. Sci. Spectrosc.* 2003; **48**: 125.
8. Kneipp K, Kneipp H, Itzkan I, Dasari RR, Feld MS. *Curr Sci India* 1999; **77**: 915.
9. Kneipp K, Kneipp H, Itzkan I, Dasari RR, Feld MS. *Chem. Rev.* 1999; **99**: 2957.
10. Kneipp K, Kneipp H, Bohr HG. *Top. Appl. Phys.* 2006; **103**: 261.
11. Bell SEJ, Mackle JN, Sirimuthu NMS. *Analyst* 2005; **130**: 545.
12. Sackmann M, Materny A. *J. Raman Spectrosc.* 2006; **37**: 305.
13. Shafer-Peltier KE, Haynes CL, Glucksberg MR, Van Duyne RP. *J. Am. Chem. Soc.* 2003; **125**: 588.
14. Shadi IT, Chowdhry BZ, Snowden MJ, Withnall R. *Spectrochim. Acta, Part A* 2003; **59**: 2213.
15. Wang TL, Chiang HK, Lu HH, Peng FY. *Opt. Quant. Electron.* 2005; **37**: 1415.
16. Stosch R, Henrion A, Schiel D, Guttler B. *Anal. Chem.* 2005; **77**: 7386.
17. Zhang DM, Xie Y, Deb SK, Davison VJ, Ben-Amotz D. *Anal. Chem.* 2005; **77**: 3563.
18. Dick LA, McFarland AD, Haynes CL, Van Duyne RP. *J. Phys. Chem. B* 2002; **106**: 853.
19. Litorja M, Haynes CL, Haes AJ, Jensen TR, Van Duyne RP. *J. Phys. Chem. B* 2001; **105**: 6907.
20. Sauer G, Brehm G, Schneider S. *J. Raman Spectrosc.* 2004; **35**: 568.
21. Hu JW, Zhao B, Xu WQ, Fan YG, Li B, Ozaki Y. *Langmuir* 2002; **18**: 6839.
22. Leyton P, Sanchez-Cortes S, Garcia-Ramos JV, Domingo C, Campos-Vallette M, Saitz C, Clavijo RE. *J. Phys. Chem. B* 2004; **108**: 17484.
23. Canamares MV, Sevilla P, Sanchez-Cortes S, Garcia-Ramos JV. *Biopolymers* 2006; **82**: 405.
24. Kneipp K, Kneipp H. *Biophys. J.* 2005; **88**: 365A.
25. Kneipp K, Kneipp H, Itzkan I, Dasari RR, Feld MS. *J. Phys. Condens. Matter.* 2002; **14**: R597.
26. Bar G, Rubin S, Cutts RW, Taylor TN, Zawodzinski TA. *Langmuir* 1996; **12**: 1172.
27. Wang YL, Chen HJ, Dong SJ, Wang E. *J. Raman Spectrosc.* 2007; **38**: 515.
28. Oldenburg SJ, Averitt RD, Westcott SL, Halas NJ. *Chem. Phys. Lett.* 1998; **288**: 243.
29. Wang J, Zhu T, Song JQ, Liu ZF. *Thin Solid Films* 1998; **329**: 591.
30. Pristinski D, Tan SL, Erol M, Du H, Sukhishvili S. *J. Raman Spectrosc.* 2006; **37**: 762.
31. Westcott SL, Oldenburg SJ, Lee TR, Halas NJ. *Langmuir* 1998; **14**: 5396.
32. Leopold N, Lendl B. *J. Phys. Chem. B* 2003; **107**: 5723.
33. Kirk CT. *Phys. Rev. B* 1988; **38**: 1255.
34. Tsu DV, Lucovsky G, Davidson BN. *Phys. Rev. B* 1989; **40**: 1795.
35. Jiang J, Bosnick K, Maillard M, Brus L. *J. Phys. Chem. B* 2003; **107**: 9964.